Kinetics and Mechanism of Iron(III) Complexation by Ferric Binding Protein: The Role of Phosphate†

Mario Gabričević,‡ Damon S. Anderson,§ Timothy A. Mietzner,§ and Alvin L. Crumbliss*,‡

Department of Chemistry, Duke University, Box 90346, Durham, North Carolina 27708-0346, and Department of Molecular Genetics and Biochemistry, University of Pittsburgh School of Medicine, Pittsburgh, Pennsylvania 15261

Received December 9, 2003; Revised Manuscript Received March 8, 2004

ABSTRACT: Iron transport across the periplasmic space to the cytoplasmic membrane of certain Gram-negative bacteria is mediated by a ferric binding protein (Fbp). This requires Fe^{3+} loading of Fbp at the inner leaflet of the outer membrane. A synergistic anion is required for tight Fe^{3+} sequestration by Fbp. Although phosphate fills this role in the protein isolated from bacterial cell lysates, nitrilotriacetate anion (NTA) can also satisfy this requirement in vitro. Here, we report the kinetics and mechanism of Fe^{3+} loading of Fbp from $Fe(NTA)_{aq}$ in the presence of phosphate at pH 6.5. The reaction proceeds in four kinetically distinguishable steps to produce $Fe^{3+}Fbp(PO_4)$ as a final product. The first three steps exhibit half-lives ranging from ca. 20 ms to 0.5 min, depending on the concentrations, and produce $Fe^{3+}Fbp(NTA)$ as an intermediate product of significant stability. The rate for the first step is accelerated with an increasing phosphate concentration, while that of the third step is retarded by phosphate. Conversion of $Fe^{3+}Fbp(NTA)$ to $Fe^{3+}Fbp(PO_4)$ in the fourth step is a slow process (half-life ∼ 2 h) and is facilitated by free phosphate. A mechanism for the Fe^{3+}-loading process is proposed in which the synergistic anions, phosphate and NTA, play key roles. These data suggest that not only is a synergistic anion required for tight Fe^{3+} sequestration by Fbp, but also the synergistic anion plays a critical role in the process of inserting Fe^{3+} into the Fbp binding site.

We are investigating the mechanism of the ferric binding protein (FbpA)-mediated[1] iron transport in pathogenic *Neisseria* spp. (*N. gonorrheae* and *N. meningitidis*) and other Gram-negative bacteria. For pathogenic *Neisseria* spp., iron transport from human-serum transferrin, docked at outer membrane receptors, into the periplasm is facilitated by FbpA that functions as a periplasmic binding protein (*1*, *2*). An investigation of the mechanism for this process is of importance, because acquisition of growth-essential iron from the infected host is related to virulence. A fundamental understanding of iron transport may provide a basis for the control of disease mediated by pathogenic *Neisseria* spp. and extrapolated to other microbial pathogens (*1*).

Two hypotheses that are relevant to the mechanism of FbpA-mediated periplasmic iron transport are currently being explored by our laboratories. In the first hypothesis, iron released from receptor-docked transferrin is assisted by $Fe^{3+} \rightarrow Fe^{2+}$ reduction and subsequent sequestration by FbpA occurs at the inner leaflet of the outer membrane, followed by reoxidation to Fe^{3+} (*3*, *4*). In the second hypothesis, iron removal from transferrin, transported across the outer membrane, and sequestration by Fbp proceed without change in the iron (+3) oxidation state. In both hypotheses, a synergistic anion associated with the binding site plays an important structural and thermodynamic role in iron binding and release by FbpA.

FbpA is a mono-lobal protein of 35 kDa with a single iron binding site between two domains. In the crystal structure of the wild-type recombinant form of iron-loaded FbpA, water and monodentate phosphate ligands are bound in the first coordination shell of Fe^{3+} (*5*). The presence of this synergistic phosphate anion is required for tight Fe^{3+} sequestration by FbpA ($K_b = 10^{18}$ M^{-1} in the presence of phosphate) (*3*). This is also the case for mammalian transferrin, where carbonate serves as the synergistic anion required for iron sequestration (*6*). FbpA exhibits a binding-site tertiary structure similar to that of mammalian transferrin, as well as similar coordinating amino acid side chains (two tyrosines, a histidine, and a glutamate for FbpA and two tyrosines, a histidine, and an aspartate for mammalian transferrin) (*5*, *7*, *8*). In addition to the structural similarities between FbpA and the transferrins, FbpA is also functionally similar to mammalian transferrin because both proteins transport tightly bound iron between membrane receptors in vivo.

A structural role for phosphate in the apo form of FbpA is supported by the presence of a phosphate anion associated with the anion binding site in the crystal structure of apo

† Financial support from the National Science Foundation (Grants CHE-0079066 and DGE-0209592 to A.L.C.) and the National Institutes of Health Grant (R29A132226 to T.A.M.) is gratefully acknowledged.

* To whom correspondence should be addressed: Department of Chemistry, Duke University, Box 90346, Durham, NC 27708-0346. E-mail: alvin.crumbliss@duke.edu. Fax: 919-660-1605.

‡ Duke University.

§ University of Pittsburgh School of Medicine.

[1] Abbreviations: Fbp, ferric iron-binding protein, is used throughout the paper to indicate nFbpA or FbpA, the recombinant protein used for these studies; unless specifically indicated, these terms should be used synonymously; hFbp, Fbp from *Haemophilius influenzae*; nFbp, recombinant Fbp from *Neisseria meningitidis*; NTA, nitrilotriacetate anion; Desferrioxamine B, $CH_3C(O)N(OH)(CH_2)_5NHC(O)(CH_2)_2C(O)N(OH)(CH_2)_5NHC(O)(CH_2)_2C(O)N(OH)(CH_2)_5NH_3)^+$; Ferrioxamine B, $Fe(CH_3C(O)N(O)(CH_2)_5NHC(O)(CH_2)_2C(O)N(O)(CH_2)_5NHC(O)(CH_2)_2C(O)N(O)(CH_2)_5NH_3)^+$.

10.1021/bi036217y CCC: $27.50
Published on Web 04/23/2004

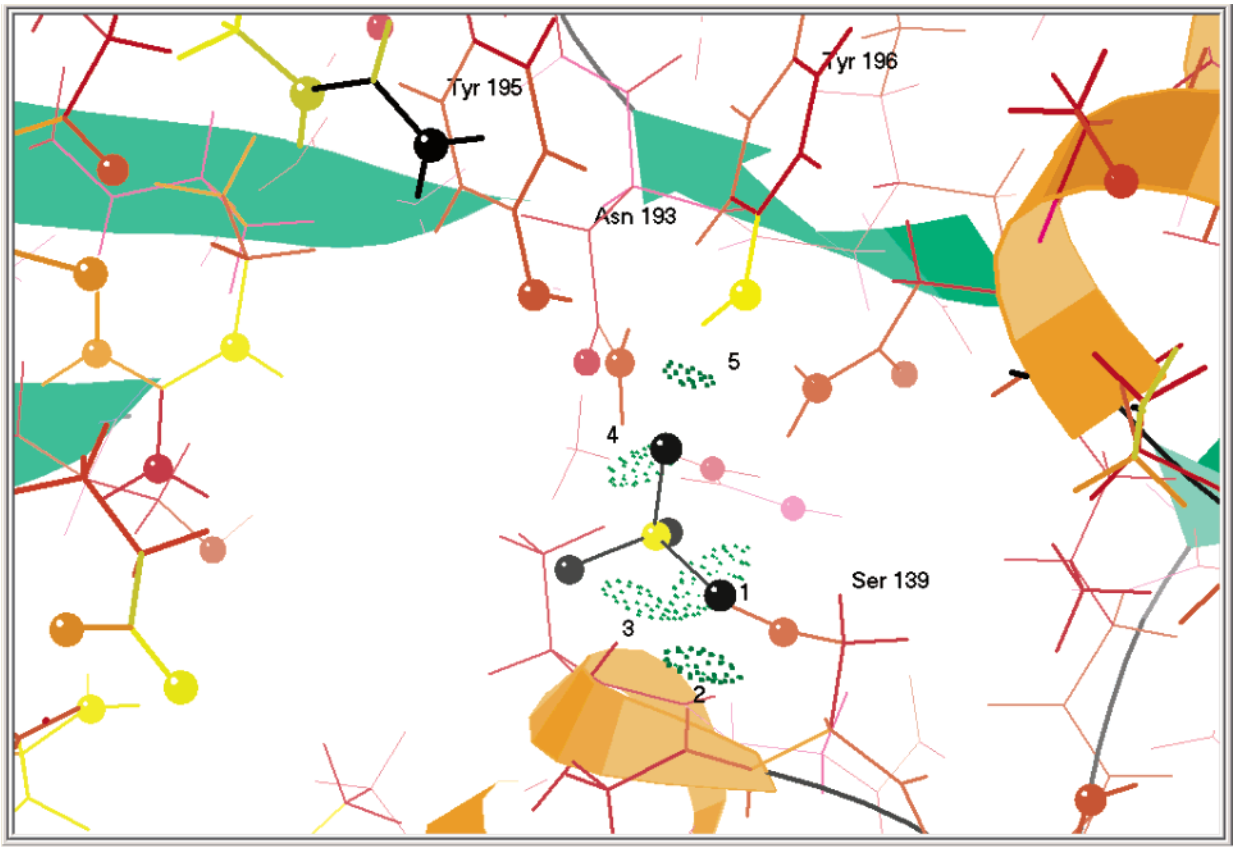

FIGURE 1: Anion binding site in C-terminal domain of apo hFbp. Probable hydrogen-bonding interactions with phosphate with distances in angstroms are as follows: (1) Ser 139 OH, 1.627; (2) Gly 140 backbone NH, 1.926; (3) Ala 141 backbone NH, 1.972; (4) Asn 193 NH, 1.983; (5) Tyr 196 OH, 2.192. Data obtained from PDB 1D9V and the model formulated using Prekin and Mage (*28*) and Reduce and Probe (*29*).

hFbp (*9*). The PO_4^{3-} anion is within hydrogen-bonding distance of several residues of the anion-binding helix as well as tyrosine 196, a residue utilized in Fe^{3+} binding. This is illustrated in Figure 1, on the basis of the crystal structure of apo hFbpA. This result has led us to postulate that the presence of the phosphate anion serves to preorganize the C-terminal binding-site domain for iron binding. On the basis of a comparison of the crystal structures for the apo and holo forms of Fbp, we may conclude that the N-terminal binding-site domain reorganizes upon Fe^{3+} binding and the two domains clamp shut with a 21° rotation about the central interdomain hinge (*5*, *9*).

In this paper, we report the kinetics and mechanism of Fe^{3+} insertion into Fbp via a nonredox process mediated by the exogenous anion, phosphate. Our kinetic results expand on the structural (*5*, *9*) and thermodynamic (*3*, *4*) roles previously identified for the phosphate synergistic anion and have important implications in the mechanism of iron loading into Fbp. Results reported here complement our recent Fbp-kinetics study that identified the importance of the synergistic anion in the proton-driven dissociation of Fe^{3+} (*10*). The significance of our solution-kinetics studies is enhanced by the fact that Fbp is one of the few periplasmic binding proteins whose solid-state structure is known for both the liganded (holo) and free (apo) states of the protein (*5*, *9*). Our kinetic studies represent a "real-time" investigation of the dynamic processes that occur between these two solid-state structures.

EXPERIMENTAL PROCEDURES

Materials. Deionized water was used in all experiments. Stock solutions of NaOH (Fisher Chemicals), nitrilotriacetic acid trisodium salt monohydrate (Acros), MES (Sigma−Aldrich), acetohydroxamic acid (Sigma−Aldrich), and Na_2HPO_4 (Sigma−Aldrich) were used without further purification. Desferrioxamine B solutions were prepared from the recrystallized mesylate salt. A stock solution of $NaClO_4$ was prepared from anhydrous $NaClO_4$ (Sigma−Aldrich), filtered, and standardized by passage through a DOWEX 50W-X8 strong acid cation exchange column in the H^+ form by titration against standard NaOH to the phenolphthalein end point. A $Fe(NTA)_{aq}$ working solution was prepared by slow addition of the appropriate volume of an acidic $Fe(ClO_4)_3$ stock solution (0.087 M $Fe(ClO_4)_3$/0.1 M $HClO_4$) to a vigorously stirred solution of nitrilotriacetic acid trisodium salt monohydrate (NTA) in MES buffer (final molar ratio of Fe^{3+}:NTA = 1:1.05). A MES buffer (50 mM) at pH 6.5 and $I = 0.15$ ($NaClO_4$) was used in all experiments. All $Fe(NTA)_{aq}$ working solutions (0.4−4 mM) were allowed to stabilize >1 h after preparation prior to use. Recombinant Fbp was prepared by a variation of the previously described method (*11*). In all kinetic experiments probing phosphate dependence, phosphate was present in both Fbp and $Fe(NTA)_{aq}$ solutions prior to mixing.

Physical Measurements. Spectral studies were performed using a Varian Cary 100-Bio UV−Vis spectrophotometer

Scheme 1

$$\text{Fbp} + \text{H}_x\text{PO}_4^{y-} + \text{Fe(NTA)}_{aq} \xrightarrow[\text{STEP I}]{k_I(0.02\,s)} \text{P}_I \xrightarrow[\text{STEP II}]{k_{II}(1\,s)} \text{P}_2 \xrightarrow[\text{STEP III}]{k_{III}(35\,s)} \text{P}_3 \xrightarrow[\text{STEP IV}]{k_{IV}(2\,h)} \text{P}_4$$

Scheme 2

$$\text{Fe(NTA)(H}_2\text{O)}_2 \underset{+\text{H}^+}{\overset{K_{a1}}{\rightleftharpoons}} \text{Fe(NTA)(H}_2\text{O)(OH)}^- \underset{+\text{H}^+}{\overset{K_{a2}}{\rightleftharpoons}} \text{Fe(NTA)(OH)}_2^{2-}$$

$$\text{H}_x\text{PO}_4^{y-} \downarrow k_1 \qquad\qquad \text{H}_x\text{PO}_4^{y-} \downarrow k_2$$

$$\text{Fe(NTA)(H}_2\text{O)(H}_x\text{PO}_4)^{y-} \underset{+\text{H}^+}{\overset{K_{a3}}{\rightleftharpoons}} \text{Fe(NTA)(OH)(H}_x\text{PO}_4)^{z-}$$

and Applied Photophysics stopped-flow (SX.18 MV) equipped with a diode array spectrophotometer with an approximate range of 380−750 nm for rapid-scan measurements. Kinetic studies were performed using an Applied Photophysics stopped-flow spectrophotometer (SX.18 MV) in absorbance and fluorescence mode at 463 and 280 nm, respectively. Data were analyzed using Applied Photophysics kinetic software. Reactions were monitored in both time-resolved fluorescence and absorbance modes, with equivalent values of k_{obs} obtained for both detection modes. All kinetic data illustrated in the figures are from fluorescence measurements and were performed under pseudo-first-order conditions of excess Fe(NTA)$_{aq}$, at 25°C, pH 6.5, and I = 0.15 ($NaClO_4$). Buffer pH adjustments were made using an Orion pH-meter model 230 A. Each kinetic data point in the figures represents an average of 3−7 replicate runs. Estimated errors are less than the data-point size.

RESULTS

General Observations. The kinetics of delivery of Fe^{3+} to Fbp were investigated at pH 6.5, the estimated pH of the periplasm where the protein resides in vivo (*12*). This necessitates using chelated Fe^{3+} to prevent hydrolysis and precipitation. Fe(NTA)$_{aq}$ was selected as an Fe^{3+} chelate source to load Fbp because of its well-characterized aqueous-solution chemistry (*13*, *14*) and wide use in mammalian-transferrin-loading experiments. The overall reaction investigated is that shown in eq 1. The exchange of Fe^{3+} from

$$\text{Fbp} + \text{H}_x\text{PO}_4^{y-} + \text{Fe(NTA)}_{aq} \rightarrow \text{FeFbpPO}_4 + \text{NTA} \quad (1)$$

Fe(NTA)$_{aq}$ to Fbp at pH 6.5 proceeds in four kinetically distinguishable steps as illustrated in Scheme 1. The numbers in parentheses represent the half-time of each kinetic step when [Fe(NTA)$_{aq}$] = 0.1 mM, [$H_xPO_4^{y-}$] = 1 mM, and [Fbp] = 7 μM. P$_x$ (x = 1−4) represents the product of each step.

After mixing solutions containing Fe(NTA)$_{aq}$ and phosphate, the equilibria in Scheme 2 are rapidly established (*14*). Equilibrium data show that at our experimental conditions (pH 6.5) only one phosphate molecule is bound per molecule of Fe(NTA)$_{aq}$ (*14*) and >90% is present as the ternary complex Fe(NTA)(OH)(H$_x$PO$_4$)$^{z-}$ (*15*).

Figure 2A represents quasi-equilibrium absorbance spectra for Steps I−III (P$_1$, P$_2$, and P$_3$) and the final product Step IV (P$_4$) illustrated in Scheme 1. Spectrum P$_3$ with λ_{max} = 465 nm corresponds to that observed for FeFbp(NTA) prepared independently (also shown in Figure 2A), while spectra P$_1$ and P$_2$ exhibit λ_{max} ~ 465 nm but with different absorbancies suggesting related but distinct species. Subsequently, in Step IV after a few hours, λ_{max} is shifted to 480

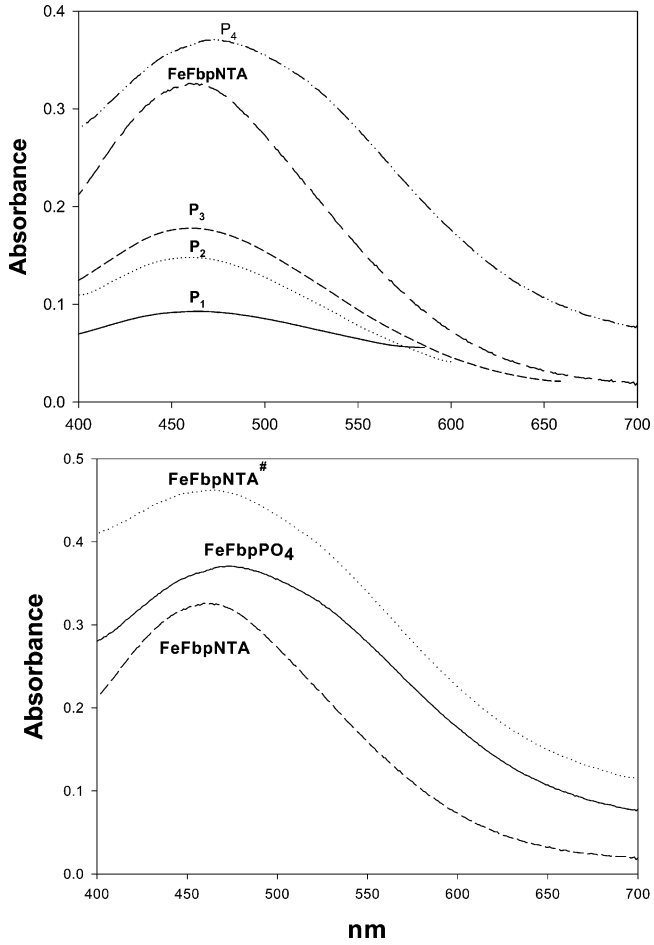

FIGURE 2: (A) Absorbance spectra corresponding to quasi-equilibrium species P$_1$, P$_2$, P$_3$, and the final product P$_4$ in Scheme 1. Conditions: [Fe(NTA)]$_{tot}$ = 0.1 mM, [Fbp] = 50 μM, [$H_xPO_4^{y-}$] = 1.0 mM, [MES] = 50 mM at pH 6.5, I = 0.15 ($NaClO_4$). Quasi-equilibrium spectra were obtained by choosing the appropriate spectrum from rapid-scan measurements after each kinetic step using the Applied Photophysics SX.18 stopped-flow diode array spectrophotometer. The spectrum labeled FeFbpNTA was obtained by mixing equal concentrations of Fbp and Fe(NTA)$_{aq}$ and equilibrating for 30 min, filtering, and diluting to give the following final conditions: [FeFbpNTA] = 70 μM, [MES] = 50 mM at pH 6.5, I = 0.15 ($NaClO_4$). (B) Bottom spectrum: FeFbp(NTA) was obtained by mixing equal concentrations of Fbp and Fe(NTA)$_{aq}$ and equilibrating for 30 min, followed by filtration and dilution. Conditions: [Fe(NTA)]$_{tot}$ = [Fbp] = 70 μM, [MES] = 50 mM at pH 6.5, I = 0.15 ($NaClO_4$). Middle spectrum: FeFbp(PO$_4$) was obtained by adding $H_xPO_4^{y-}$ to FeFbp(NTA) and equilibrating for ~4 h. Conditions: [Fe^{3+}]$_{tot}$ = 70 μM, [MES] = 50 mM, [$H_xPO_4^{y-}$] = 5 mM at pH 6.5, I = 0.15 ($NaClO_4$). Top spectrum: FeFbpNTA$^{\#}$ was obtained by adding NTA to Fe−Fbp−PO$_4$ and equilibrating for ~2 h. Conditions: [Fe^{3+}]$_{tot}$ = 100 μM, [NTA]$_{tot}$ = 500 μM, [MES] = 50 mM at pH 6.5, I = 0.15 ($NaClO_4$).

Scheme 3 [a]

$$\mathrm{Fbp} + \mathrm{H_xPO_4^{y-}} \rightleftharpoons \mathrm{Fbp\text{-}PO_4} \qquad K_1 \quad (2)$$

$$\mathrm{Fe(NTA)} + \mathrm{H_xPO_4^{y-}} \rightleftharpoons \mathrm{Fe(NTA)(H_xPO_4)^{y-}} \qquad K_2 \quad (3)$$

$$\mathrm{Fbp\text{-}PO_4} + \mathrm{Fe(NTA)(H_xPO_4)^{y-}} \underset{k_{-3},k_{-3}'}{\overset{k_3}{\rightleftharpoons}} \mathrm{Fe(NTA)(Fbp\text{-}PO_4)^{*}} + \mathrm{H_xPO_4^{y-}} \qquad K_3 \quad (4)$$

$$\mathbf{P_1}$$

$$\mathrm{Fe(NTA)(Fbp\text{-}PO_4)^{*}} \underset{k_{-4}}{\overset{k_4}{\rightleftharpoons}} \mathrm{Fe(NTA)(Fbp\text{-}PO_4)^{**}} \qquad K_4 \quad (5)$$

$$\mathbf{P_2}$$

$$\mathrm{Fe(NTA)(Fbp\text{-}PO_4)^{**}} \rightleftharpoons \mathrm{Fe(NTA)(Fbp)^{*}} + \mathrm{H_xPO_4^{y-}} \qquad K_5 \quad (6)$$

$$\mathrm{Fe(NTA)(Fbp)^{*}} \xrightarrow{k_6} \mathrm{Fe(Fbp)(NTA)} \qquad (7)$$

$$\mathbf{P_3}$$

$$\mathrm{Fe(Fbp)(NTA)} + \mathrm{H_xPO_4^{y-}} \longrightarrow \mathrm{Fe(Fbp)(NTA)^{**}} \longrightarrow \mathrm{Fe(Fbp)(PO_4)} + \mathrm{NTA} \qquad (8)$$

$$\mathbf{P_4}$$

Step I, Step II, Step III, Step IV

[a] Water ligands are not shown for simplicity. Species marked with a single and double asterisk represent the transient kinetic intermediates that are not isolated. Tentative structures are illustrated in Scheme 5.

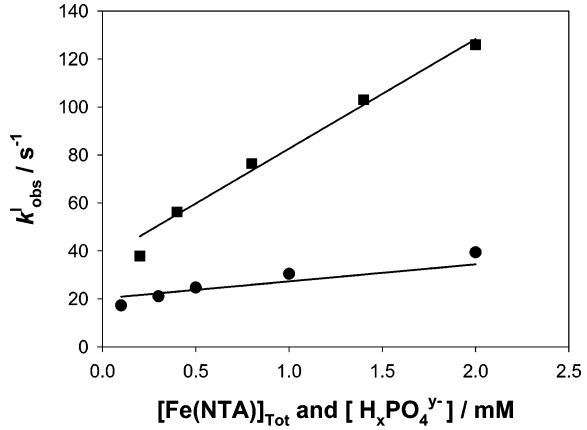

FIGURE 3: k^{I}_{obs} versus $[H_xPO_4^{y-}]$ (●) and $[Fe(NTA)]_{tot}$ (*15*) (■) for Step I (Scheme 1) of eq 1. Conditions: (●), $[FeNTA]_{tot} = 0.1$ mM, [Fbp] = 7 μM at pH 6.5, $I = 0.15$ ($NaClO_4$) at 25 °C. (■), $[H_xPO_4^{y-}] = 5$ mM, [Fbp] = 7 μM at pH 6.5, $I = 0.15$ ($NaClO_4$) at 25 °C. In both cases, the solid line represents a fit of eq 10 to the data.

nm, which corresponds to the phosphate substitution of NTA to give FeFbp(PO_4) (P_4 spectrum, Figure 2A) (*16*). Step IV is reversible as illustrated in Figure 2B, where the spectrum of FeFbp(NTA) is generated by reacting FeFbp(PO_4) with NTA and vice versa.

Evidence for the pivotal role of phosphate in the Fe^{3+} insertion reaction can be deduced by the observation that in the absence of phosphate the rates are significantly altered and only two steps corresponding to Steps II and III in Scheme 1 are observed (see results associated with Scheme 4 as described below).

Kinetic Data in the Presence of Phosphate. Our working model for the overall process described in eq 1 and Scheme 1 is illustrated in Scheme 3, where Step I in Scheme 1 corresponds to eqs 2−4, Step II, to eqs 2−5, Step III, to eqs 6 and 7, and Step IV, to eq 8.

In Step I (eqs 2−4), the observed pseudo-first-order rate constant (k^{I}_{obs}) is dependent on both phosphate and Fe(NTA)$_{tot}$ concentrations (Figure 3). Increasing the concentration of phosphate or Fe(NTA)$_{tot}$ results in an increased change in the fluorescence signal amplitude, indicating a shift of the equilibrium toward the products represented as P_1. Consequently, the intercept in Figure 3 may be attributed to the back reaction, which is represented as the reverse of eq 4. Because both Fe(NTA)$_{aq}$ and Fbp react with phosphate ions producing $FbpPO_4$ and a ternary Fe^{3+} complex $Fe(NTA)(OH)(H_xPO_4)^{y-}$ (*9*, *14*, *15*, *17*), a mechanism for Step I can be written as depicted in eqs 2−4 in Scheme 3. At pseudo-first-order conditions ($[Fe^{3+}] \gg [Fbp]$) and assuming eqs 2 and 3 are rapid preequilibria to the rate-determining eq 4, we obtain eq 9. Because K_2 is relatively

$$k^{I}_{obs} = \frac{k_3K_1K_2[H_xPO_4^{y-}]^2[Fe(NTA)]_{tot}}{1 + (K_1 + K_2)[H_xPO_4^{y-}] + K_1K_2[H_xPO_4^{y-}]^2} + k_{-3}[H_xPO_4^{y-}] + k'_{-3} \quad (9)$$

large ($\log K_2 = 6.84$) (*17*) and, at our experimental conditions >90% (in most cases >95%) of Fe(NTA)$_{aq}$, is in the Fe−NTA−phosphate form, eq 9 can be further simplified to eq 10 (*15*). A fit of eq 10 to the experimental data in Figure 3

$$k^{I}_{obs} = \frac{k_3K_1[H_xPO_4^{y-}]}{1 + K_1[H_xPO_4^{y-}]}[Fe(NTA)]_{tot} + k_{-3}[H_xPO_4^{y-}] + k'_{-3} \quad (10)$$

while holding K_1 constant at its literature value ($K_1 = 4.2 \times 10^2$ M^{-1}) (*9*) produces the values for parameters k_3, k_{-3}, and k'_{-3} listed in Table 1. We can eliminate phosphate-free Fbp and Fe(NTA)$_{aq}$ as a reactive species in Step I because of a poor fit of the derived rate expressions to the experimental data when they are included.

The data in Figure 4 illustrate the variation of the observed rate constant (k^{II}_{obs}) with respect to both the Fe(NTA)$_{tot}$ and phosphate concentrations for Step II (Scheme 1). If we consider that eqs 2−4 are rapid preequilibria to eq 5 (the rate-determining reaction in Step II), eq 11 can be derived. Equation 11 was fit to the data presented in Figure 4A to

$$k^{II}_{obs} = \frac{k_4K_1K_3[Fe(NTA)]_{tot}}{1 + K_1[H_xPO_4^{y-}] + K_1K_3[Fe(NTA)]_{tot}} + k_{-4} \quad (11)$$

Table 1: Microscopic Rate and Equilibrium Constants

parameter	equation number	value[a]	comment
K_1	2, 9, 10	4.2×10^2 M^{-1}	*b*
K_2	3, 9	6.9×10^6 M^{-1}	*c*
k_3	4, 9, 10	$3.6(0.2) \times 10^4$ M^{-1} s^{-1}	*d*
K_3	4, 11	$1.5(0.8) \times 10^2$	*e*
k_{-3}	4, 9, 10	$5.2(1.5) \times 10^3$ M^{-1} s^{-1}	*d*
k'_{-3}	4, 9, 10	$2.0(0.3) \times 10^1$ s^{-1}	*d*
k_4	5, 11	$0.52(0.08)$ s^{-1}	*e*
k_{-4}	5, 11	$0.3(0.1)$ s^{-1}	*e*
K_5	6, 12	$3.0(0.3) \times 10^{-3}$ M	*f*
k_6	7, 12	$2.47(0.05) \times 10^{-2}$ s^{-1}	*f*
k_7	14, 16	$2.6(0.1) \times 10^3$ M^{-1} s^{-1}	*g*
k_{-7}	14, 16	$0.24(0.03)$ s^{-1}	*g*
k_8	15	$2.2(0.1) \times 10^{-2}$ s^{-1}	*h*

[a] Number in parentheses denotes the standard deviation. [b] ref 9. [c] ref 17. [d] Value was obtained from a fit of eq 10 to the data (Figure 3), where K_1 was fixed at 4.2×10^2 M^{-1}. [e] Value was obtained from a fit of eq 11 to the data (Figure 4A). [f] Value was obtained from a fit of eq 12 to the data (Figure 5A). [g] Value was obtained from a fit of eq 16 to the data (Figure 6). [h] Value was obtained from the data in Figure 6.

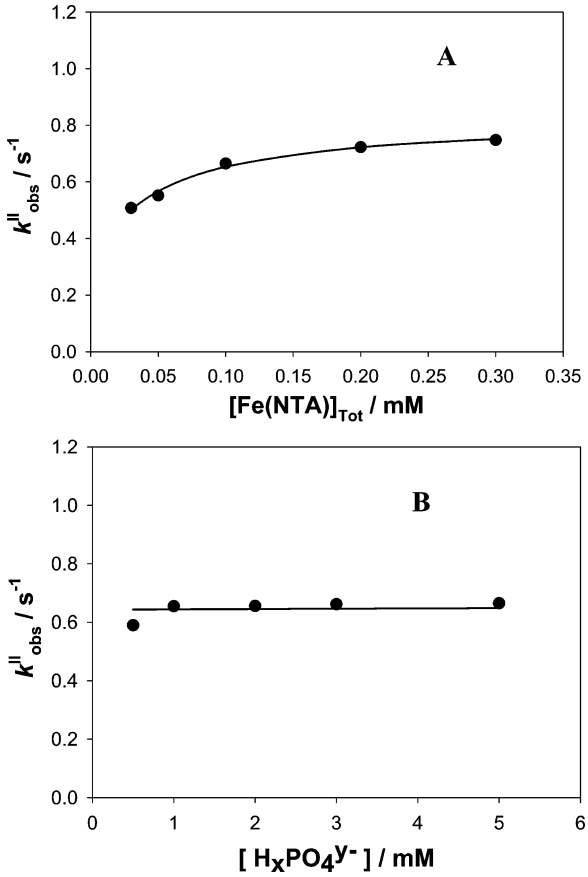

FIGURE 4: (A) k^{II}_{obs} versus $[Fe(NTA)]_{tot}$ for Step II (Scheme 1) of eq 1. Conditions: $[H_xPO_4^{y-}] = 5$ mM, [Fbp] = 7 μM at pH 6.5, $I = 0.15$ ($NaClO_4$) at 25 °C. The solid line represents a fit of eq 11 to the data. (B) k^{II}_{obs} versus $[H_xPO_4^{y-}]$ for Step II (Scheme 1) of eq 1. Conditions: $[Fe(NTA)]_{tot} = 0.2$ mM, [Fbp] = 7 μM at pH 6.5, $I = 0.15$ ($NaClO_4$) at 25 °C. The solid line represents a fit of eq 11 to the data at the experimental conditions, where $k^{II}_{obs} \approx k_4 + k_{-4}$; see the text.

obtain values for k_4, k_{-4}, and K_3, which are listed in Table 1 for the case where K_1 was held constant at its previously reported value (*9*). Treating K_1 as an adjustable parameter yields a value consistent with that previously reported in the literature and comparable values for k_4, k_{-4}, and K_3, although

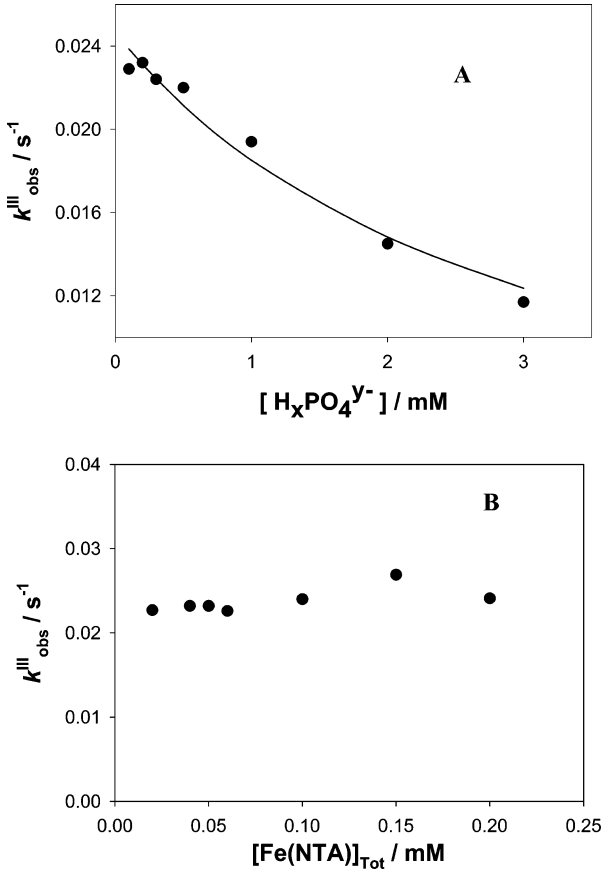

FIGURE 5: (A) k^{III}_{obs} versus $[H_xPO_4^{y-}]$ for Step III (Scheme 1) of eq 1. Conditions: $[Fe(NTA)]_{tot} = 0.1$ mM, [Fbp] = 7 μM at pH 6.5, $I = 0.15$ ($NaClO_4$). The solid line represents a fit of eq 12 to the data. (B) k^{III}_{obs} versus $[Fe(NTA)]_{tot}$ (*15*) for Step III (Scheme 1) of eq 1. Conditions: $[H_xPO_4^{y-}] = 0.5$ mM, [Fbp] = 7 μM at pH 6.5, $I = 0.15$ ($NaClO_4$) at 25 °C.

with larger standard deviations. At the conditions of the variable phosphate kinetic experiments shown in Figure 4B, the denominator in the first term of eq 11 is dominated by the $K_1K_3[Fe(NTA)]_{tot}$ term and consequently eq 11 simplifies to $k^{II}_{obs} \approx k_4 + k_{-4}$. The constant value observed for k^{II}_{obs} in Figure 4B (0.64 s^{-1}) is consistent with the sum of k_4 and k_{-4} obtained from a fit of eq 11 to the data in Figure 4A, within experimental error.

In Step III (Scheme 1), k^{III}_{obs} was found to be inversely dependent on the phosphate concentration and independent of the $[Fe(NTA)]_{tot}$ concentration (Figure 5). The simplest mechanism consistent with these data is depicted in eqs 6 and 7 (Scheme 3), where eq 6 is a rapid equilibrium step prior to eq 7, and the rate law is depicted in eq 12. A fit of eq 12 to the data in Figure 5 yields the k_6 and K_5 parameters listed in Table 1. Including a term for the reverse of eq 7

$$k^{III}_{obs} = \frac{k_6 K_5}{K_5 + [H_xPO_4^{y-}]} \qquad (12)$$

did not improve the fit. Consequently, we conclude that at our experimental conditions the back reaction in Step III is negligible.

The product of Step III is the NTA form of iron−Fbp, FeFbp(NTA), where NTA is the synergistic anion required for tight iron binding. This is established by the spectra shown in Figure 2, which are consistent with our previous

Scheme 4

$$\text{Fbp} + \text{Fe(NTA)}_{aq} \xrightarrow[\text{STEP Ia}]{k_{Ia}(1\,s)} P_{1a} \xrightarrow[\text{STEP IIa}]{k_{IIa}(30\,s)} P_{2a}$$

observations (*4*). In Step IV, the phosphate anion slowly exchanges with NTA in two stages to produce FeFbp(PO_4) as the final product. The kinetics and mechanism of Step IV as illustrated in the anion exchange reaction (eq 8) will be reported in detail elsewhere (*18*), because the focus of this paper is the phosphate-anion-assisted insertion of Fe^{3+} into apo Fbp.

Other Relevant FeNTA$_{aq}$ Ligation Reactions in the Presence of Phosphate. To evaluate the uniqueness of the phosphate dependence observed in the exchange of Fe^{3+} between NTA and Fbp (eq 1), we investigated the influence of the phosphate ion on the kinetics of eq 13 at pH 6.5, where L = acetohydroxamic acid or desferrioxamine B (H_4DFB^+),

$$\text{Fe(NTA)}_{aq} + \text{L} \rightarrow \text{FeL} + \text{NTA}^{3-} \qquad (13)$$

and FeL represents tris(acetohydroxamato)iron(III) (Fe($CH_3C(O)N(O)H)_3$) or ferrioxamine B ($FeHDFB^+$). Proton stoichiometries are omitted for simplicity. The reaction conditions were $[Fe(NTA)]_{tot}$ = 0.1 mM, [L] = 1 mM, [MES] = 50 mM, I = 0.15 ($NaClO_4$), and pH 6.5. The observed pseudo-first-order rate constant for eq 13 is independent of the phosphate concentration (data not shown) up to 10 mM (100-fold molar excess over Fe(NTA)$_{aq}$) for both L = acetohydroxamic acid ($k_{obs} = 1.2 \times 10^2$ s^{-1}) or desferrioxamine B ($k_{obs} = 2.0 \times 10^1$ s^{-1}). Clearly, there is no phosphate anion effect on the kinetics of eq 13, which is strongly suggestive of a specific mechanism for the phosphate anion effect on the kinetics of Fe^{3+} exchange between $FeNTA_{aq}$ and apo Fbp (eq 1).

Fe(NTA)$_{aq}$ Reaction with Fbp in the Absence of Phosphate. To further explore the critical role of phosphate in the exchange of Fe^{3+} from Fe(NTA)$_{aq}$ to apo Fbp, we investigated the process in the absence of phosphate. In this case, only two steps appear in the formation of FeFbp(NTA), as illustrated in Scheme 4. The numbers in parentheses in Scheme 4 represent the half-time of each kinetic step at the following conditions: [Fe(NTA)$_{aq}$] = 0.1 mM, [Fbp] = 7 μM, MES = 50 mM at pH 6.5, and I = 0.15 M ($NaClO_4$). Changes in the fluorescence signal amplitudes for Steps Ia and IIa are equivalent. Spectra corresponding to the quasi-equilibrium species P_{1a} and equilibrium species P_{2a} exhibit λ_{max} at 465 nm, corresponding to FeFbp(NTA) (*4*). Fe^{3+} insertion from $FeNTA_{aq}$ into apo Fbp may be viewed as a two-step process as illustrated in eqs 14 and 15, where $FeFbpNTA^*$ represents Fe(NTA) that is only partially sequestered by Fbp. The k_{obs} values for eq 14 are linearly

$$\text{Fe(NTA)}_{aq} + \text{Fbp} \underset{k_{-7}}{\overset{k_7}{\rightleftharpoons}} \text{FeFbpNTA*} \qquad (14)$$

$$\text{FeFbpNTA*} \xrightarrow{k_8} \text{FeFbp(NTA)} \qquad (15)$$

dependent on [Fe(NTA)$_{aq}$] (Figure 6). A fit of eq 16 to the

$$k_{obs} = k_7[\text{Fe(NTA)}_{aq}] + k_{-7} \qquad (16)$$

data in Figure 6 for eq 14 yields $k_7 = 2.6(0.1) \times 10^3$ M^{-1} s^{-1} and $k_{-7} = 0.24(0.03)$ s^{-1} from the slope and intercept.

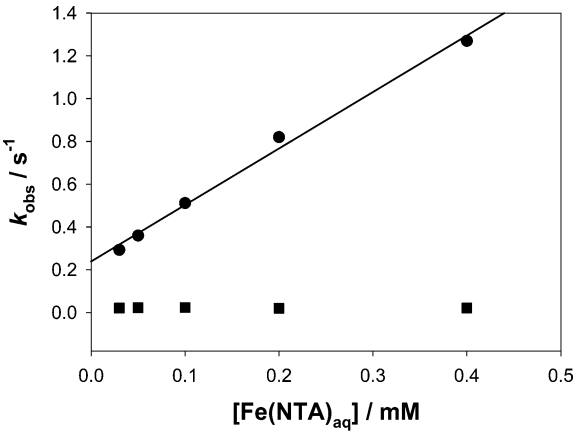

FIGURE 6: Pseudo-first-order rate constants (k_{obs}) versus [Fe(NTA)$_{aq}$] for Step Ia, eq 14, (●) and Step IIa, eq 15, (■) in Scheme 4 in the absence of phosphate. Conditions: [Fbp] = 8 μM, [MES] = 50 mM at pH 6.5, I = 0.15 ($NaClO_4$) at 25 °C. Solid line represents a linear least-squares fit of eq 16 to the data for eq 14.

The k_{obs} values for eq 15 exhibit no Fe(NTA)$_{aq}$ concentration dependence (Figure 6) and $k_8 = 2.2(0.1) \times 10^{-2}$ s^{-1}.

DISCUSSION

Results presented here clearly demonstrate that phosphate plays a role in inserting Fe^{3+} into apo Fbp from $FeNTA_{aq}$. Furthermore, this kinetic role is distinct from the thermodynamic role that phosphate plays as an exogenous anion required for the tight sequestration of Fe^{3+} by Fbp in the ternary assembly FeFbp(PO_4) (*3*, *4*). This is illustrated on a qualitative level by comparison of Schemes 1 and 4 for the Fe^{3+}-insertion process in the presence and absence of phosphate, respectively. Both processes produce FeFbp(NTA) (P_3 in Scheme 1 and P_{2a} in Scheme 4), but at different rates and in a different number of kinetically distinguishable steps. The kinetics of Scheme 1 are dependent on the phosphate concentration. An additional slow step involving exogenous anion exchange is added in the phosphate reaction to produce the more stable FeFbp(PO_4) as the final product. The unique role of phosphate in the iron Fbp insertion reaction is emphasized by the lack of phosphate influence on eq 13 involving the exchange of Fe^{3+} between NTA and acetohydroxamic acid or desferrioxamine B.

Scheme 5 is a molecular cartoon that summarizes our model for phosphate-facilitated insertion of Fe^{3+} into Fbp. In Step I (Scheme 1 and eqs 2−4), the phosphate anion facilitates the initial Fe^{3+} insertion into Fbp. This is supported by two observations: (1) the observed rate constant (k^I_{obs}) increases with increasing [$H_xPO_4^{y-}$] (Figure 3), and (2) a comparison of the second-order rate constants for the rate-determining process in the first step of Fe^{3+} insertion in the presence ($k_3 = 3.6 \times 10^4$ M^{-1} s^{-1}) and absence ($k_7 = 2.6 \times 10^3$ M^{-1} s^{-1}) of phosphate shows a phosphate anion enhancement ($k_3/k_7 \approx 15$). This rate-constant increase in the presence of phosphate suggests a catalytic role for this anion in the Fe^{3+}-insertion process. Because phosphate does not similarly enhance the reaction of Fe(NTA)$_{aq}$ with acetohydroxamic acid or desferrioxamine B (eq 13), we can deduce that this effect may be specific to the Fbp protein. Apparently, the rate acceleration effect in Step I (Figure 3) comes from a preequilibrium reaction involving phosphate and the protein

Scheme 5

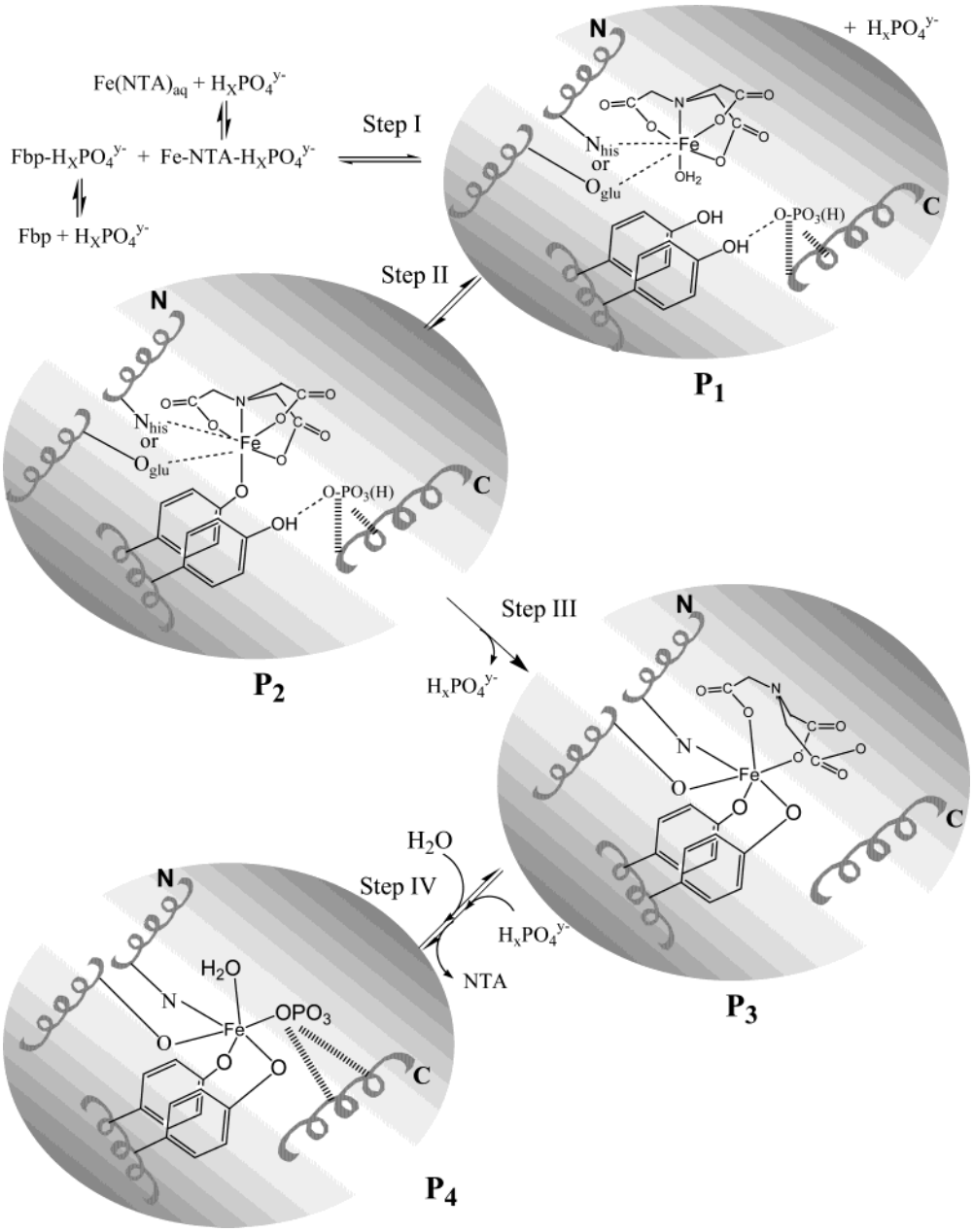

(eq 2), represented in Scheme 5 as the preorganization of tyrosines 195 and 196 in the C-terminal binding domain. This preequilibrium is consistent with the X-ray crystal structure of apo Fbp (*9*) that shows phosphate associated with the anion binding site and hydrogen bonded to tyrosine 196 as illustrated in Figure 1. Our model is further supported by the fact that when K_1 in eq 10 is treated as a variable parameter the value obtained in our data analysis is in reasonable agreement with the published value for phosphate binding to apo Fbp (*9*). The phosphate in solution may stabilize a specific protein tertiary structure by taking it from a molten globule to a defined conformation that preorganizes the C-terminal domain in a transition-state-like structure for Fe^{3+} sequestration and thus is responsible for our observation that $k_3 > k_7$.

In Scheme 5, we propose the initial $FeNTA_{aq}$ coordination to His or Glu in the binding cleft based on the observed absorbance and fluorescence amplitudes for Step I. Absorbance changes are consistent with ligation at the Fe^{3+} center. Tyrosine fluorescence will be quenched by binding or close proximity to the paramagnetic Fe^{3+} ion and hydrogen bonding or dissociation of the phenolic proton (*19*). The ratio of relative fluorescence amplitudes for Steps I−III are 10:45:45%, consistent with the initial coordination through His or Glu, rather than Tyr (data not shown). His and Glu coordination are supported by the X-ray crystal structure for holo Fbp (*5*).

The relative fluorescence amplitudes of 45% suggest direct coordination of Fe^{3+} with the two tyrosine residues in Steps II and III. The inverse phosphate ion dependence on the observed rate constant in Step III (Figure 5A) arises from the dissociation of phosphate from Fbp prior to the rate-determining (k_6) protein-binding site closure and coordination of the second tyrosine to Fe^{3+} to form FeFbp(NTA) (Scheme 5). This interpretation is consistent with $k_6 \approx k_8$ (Table 1) because both eqs 7 and 15 involve the final stage of protein closure to form FeFbp(NTA) and do not involve phosphate.

Step IV is a relatively slow exchange of a water and phosphate for NTA in fully Fe^{3+}-loaded FeFbp(NTA). The incorporation of a water ligand along with the synergistic anion in the first coordination shell of Fe^{3+} is one of the distinguishing features of Fbp relative to mammalian transferrin. Our results show that Step IV occurs in two steps involving a phosphate-independent and phosphate-dependent process.

Previous kinetic studies of mammalian transferrin investigated the role of the iron chelate and synergistic carbonate anion on the mechanisms of iron loading (*20*, *21*). The Fe^{3+} exchange reaction between tris(acetohydroxamato)iron(III) and transferrin was studied by Cowart and co-workers, who report a role for the synergistic anion carbonate that is related to that proposed here for phosphate (*22*). More recently, El Hage Chahine and co-workers (*23*) propose three kinetic steps in loading the tris(acetohydroxamato)iron(III) complex into the C-lobe site of human transferrin, on the basis of time-resolved fluorescence and absorbance data. Lindley and co-workers utilized X-ray structural data for the 18 kDa NII domain fragment of duck ovotransferrin to suggest the formation of an iron−NTA−transferrin ternary complex when iron is exchanged from $Fe(NTA)_{aq}$ to the protein (*24*).

Although FeFbp(PO_4) is the thermodynamic end product in our experiments, the fact that eq 1 in the presence of phosphate produces FeFbp(NTA) as a stable initial product suggests an important role for the amine carboxylate chelator in the Fe^{3+}-insertion process. This is consistent with the recent crystal structure of a mutant form of Fbp in which Fe^{3+} is partially sequestered by Fbp while still being tetracoordinated to EDTA (*25*, *26*).

This paper represents the time-dependent sequence of events associated with closure of the interdomain hinge, a dynamic Fe^{3+} sequestration process that induces the change in conformation between the "static" solid-state structures of apo and holo Fbp (*5*, *9*). The phosphate anion has previously been shown to influence the thermodynamics of Fe^{3+} sequestration by Fbp (*3*, *4*). An exogenous anion is required for strong complexation of Fe^{3+} at the active site, and while several anions may participate in this role (*4*, *27*), phosphate is the anion found in the protein when isolated from bacterial cultures and has been shown to produce the most stable iron-loaded form of Fbp, FeFbp(PO_4)(OH_2) (*4*). In our previous kinetics investigation, we observed that, in the proton-driven dissociation of Fe^{3+} from FeFbp(PO_4)(OH_2), protonation and dissociation of the PO_4^{3-} are initial steps in the release of iron from the protein (*10*). In this paper, we establish that phosphate also plays a pivotal kinetic role in the in vitro Fe^{3+} loading of Fbp. Whether this role extends to in vivo conditions and whether our observed phosphate behavior warrants its consideration as an anion with insertase activity remain to be established.

Careful examination of the role of the synergistic anion in the mechanism by which Fbp sequesters iron is justified because bacteria respond rapidly to changes in their environment. The periplasm, the compartment of Gram-negative bacteria that lies between the outer and cytoplasmic membranes, comprises up to 30% of the cellular volume (*12*). It is clear that polyphosphate anions accumulate in the periplasm of organisms such as *Neisseria* spp., from which Fbp was derived (*12*). In addition, a gradient of anions (e.g., lactate or acetate) derived from fermentation or from respiration (e.g., citrate, oxalate, etc.) will be present because of diffusion from the cytosol through the periplasm and into the external milieu or from diffusion through porins from the external environment into the periplasm. In either case, the periplasmic space is a complex mixture of anions that will change depending on the physiologic status of the organism. On the basis of our previous work (*4*), the composition of the anion pool will influence which anion occupies the Fbp anion binding site, which in turn may influence the ease by which iron is inserted (i.e., insertase activity) or released.

ACKNOWLEDGMENT

We thank Katherine D. Weaver, Duke University, for helpful discussions and the modeling and construction of Figure 1 and Suraj Dhungana and Kassy Mies, Duke University, for helpful discussions and assistance with the graphics.

REFERENCES

1. Mietzner, T. A., Tencza, S. B., Adhikari, P., Vaughan, K. G., and Nowalk, A. J. (1998) Fe(III) Periplasm-to-cytosol transporters of Gram-negative pathogens, *Curr. Top. Microbiol. Immunol. 225*, 114.
2. Clarke, T. E., Tari, L. W., and Vogel, H. J. (2001) Structural biology of bacterial iron uptake system, *Curr. Topics Med. Chem. 1*, 7.
3. Taboy, C. H., Vaughan, K. G., Mietzner, T. A., Aisen, P., and Crumbliss, A. L. (2001) Fe^{3+} coordination and redox properties of a bacterial transferrin, *J. Biol. Chem. 276*, 2719.
4. Dhungana, S., Taboy, C. H., Anderson, D. A., Vaughan, K. G., Aisen, P., Mietzner, T. A., and Crumbliss, A. L. (2003) The influence of the synergistic anion on iron chelation by ferric binding protein, a bacterial transferrin, *Proc. Natl. Acad. Sci. U.S.A. 100*, 3659.
5. Bruns, C. M., Nowalk, A. J., Arvail, A. S., McTigue, M. A., Vaughan, K. G., Mietzner, T. A., and McRee, D. E. (1997) Structure of Haemophilus Influenzae Fe^{3+}-binding protein reveals convergent evolution within a superfamily, *Nat. Struct. Biol. 4*, 919.
6. Aisen, P. (1998) Transferrin, the transferrin receptor, and the uptake of iron by cells, *Met. Ions Biol. Syst. 35*, 585.
7. Baker, E. N. (1994) Structure and reactivity of transferrins, *Adv. Inorg. Chem. 41*, 389.
8. Baker, E. N., and Lindley, P. F. (1992) New Perspectives on the structure and functions of transferrins, *J. Inorg. Biochem. 47*, 147.
9. Bruns, C. M., Anderson, D. S., Vaughan, K. G., Williams, P. A., Nowalk, A. J., McRee, D. E., and Mietzner, T. A. (2001) Crystallographic and biochemical analyses of the metal-free *Haemophilus influenzae* Fe^{3+}-binding protein, *Biochemistry 40*, 15631.
10. Boukhalfa, H., Anderson, D. S., Mietzner, T. A., and Crumbliss, A. L. (2003) Kinetics and mechanism of iron release from the bacterial ferric binding protein nFbp: Exogenous anion influence and comparison with mammalian transferrin, *J. Biol. Inorg. Chem. 8*, 881.
11. Mietzner, T. A., Bolan, G., Schoolnik, G. K., and Morse, S. A. (1987) Purification and characterization of the major iron-regulated protein expressed by pathogenic *Neisseriae*, *J. Exp. Med. 165*, 1041.
12. Ferguson, S. J. (1991) Periplasm in *Prokaryotic Structure and Function: A New Prespective: 47th Symposium of the Society for General Microbiology* (Mohan, S., Dow, C., and Coles, J. A., Eds.) pp 311−339, Cambridge University Press, Edinburg, U.K.
13. Motekaitis, R. J., and Martell, A. E. (1994) The iron(III) and iron(II) complexes of nitrilotriacetic acid, *J. Coord. Chem. 31*, 67.
14. Gabričević, M., and Crumbliss, A. L. (2003) Kinetics and mechanism of iron(III)−nitrilotriacetate complex reactions with phosphate and acetohydroxamic acid, *Inorg. Chem. 42*, 4098.

15. Throughout the manuscript $[Fe(NTA)]_{tot}$ represents the total nonprotein-bound Fe^{3+} reactant concentration illustrated by Scheme 2 and is greater than 90% $Fe(NTA)(OH)(H_xPO_4)^{y-}$.
16. Nowalk, A., Tencza, S., and Mietzner, T. A. (1994) Coordination of iron by the ferric ion-binding protein of pathogenic *Neisseria* is homologous to the transferrin, *Biochemistry 33*, 12769.
17. Yanez-Sedeno, P. C.-M., A., and Gallego-Andreu, R. (1986) Estudio espectrofotometrico de los complejos Fe(III)-acidio nitrilotriacetico-oxoanion, *An. Quim., Ser. B 82*, 90.
18. Gabričević, M., Anderson, D. S., Mietzner, T. A., and Crumbliss, A. L., manuscript in preparation.
19. Shimizu, O., Watanabe, J., and Imakubo, K. (1979) Effect of phosphate ion on fluorescent characteristics of tyrosine and its conjugate base, *Photochem. Photobiol. 29*, 915.
20. Aisen, P., and Leibman, A. (1973) The role of the anion-binding site of transferrin in its interaction with the reticulocyte, *Biochim. Biophys. Acta 304*, 797.
21. Baker, E. N. (1993) in *Perspectives on Bioinorganic Chemistry* (Hay, R. W., Dilworth, J. R., and Nolan, K. B., Eds.) Vol. 2, p 161, JAI Press, Greenwich, CT.
22. Cowart, R., Kojima, N., and Bates, G. (1982) The exchange of Fe(III) between acetohydroxamic acid and transferrin. Spectrophotometric evidence for a mixed ligand complex, *J. Biol. Chem. 257*, 7560.
23. Pakdaman, R., Abdallah, F. B., and El Hage Chahine, J.-M. (1999) Transferrin: Is a mixed chelate-protein ternary complex involved in the mechanism of iron uptake by serum-transferrin in vitro? *J. Mol. Biol. 293*, 1273.
24. Kuser, P., Hall, D. R., Haw, M. L., Neu, M., Evans, R. W., and Lindley, P. F. (2002) The mechanism of iron uptake by transferrin: The X-ray structures of the 18 kDa NII domain fragment of duck ovotransferrin and its nitrilotriacetate complex, *Acta Crystallogr., Sect. D 58*, 777.
25. Shouldice, S. R., Dougan, D. R., Skene, R. J., Tari, L. W., McRee, D. E., Yu, R., and Schryvers, A. B. (2003) High resolution structure of an alternate form of the ferric ion binding protein from *Haemophilus influenzae*, *J. Biol. Chem. 278*, 11513.
26. Weaver, K. D., and Crumbliss, A. L. (2003) High-resolution structure of an alternate form of the ferric ion binding protein from *Haemophilus influenzae*, *Chemtracts 16*, 715.
27. Guo, M., Harvey, I., Yang, W., Coghil, L., Campopiano, D. J., Parkinson, J. A., MacGillivray, R. T., Harris, W. R., and Sadler, P. J. (2003) Synergistic anion and metal binding to the ferric ion-binding protein from *Neisseria gonorrhoeae*, *J. Biol. Chem. 278*, 2490.
28. Richardson, D. C., and Richardson, J. S. (1994) Kinemages-Simple macromolecular graphics for interactive teaching and publication, *Trends Biochem. Sci. 19*, 135.
29. Word, J. M., Lovell, S. C., LaBean, T. H., Taylor, H. C., Zalis, M. E., Presley, B. K., Richardson, J. S., and Richardson, D. C. (1999) Visualizing and quantifying molecular goodness of fit: Small probe contact dots with explicit hydrogen atoms, *J. Mol. Biol. 285*, 1711.

BI036217Y